

## Split-gate device for indirect excitons

C. J. Dorow, J. R. Leonard, M. M. Fogler, L. V. Butov, K. W. West, and L. N. Pfeiffer

Citation: *Appl. Phys. Lett.* **112**, 183501 (2018); doi: 10.1063/1.5021488

View online: <https://doi.org/10.1063/1.5021488>

View Table of Contents: <http://aip.scitation.org/toc/apl/112/18>

Published by the [American Institute of Physics](#)

---

---

**PHYSICS TODAY**

WHITEPAPERS

### MANAGER'S GUIDE

Accelerate R&D with  
Multiphysics Simulation

READ NOW

PRESENTED BY

 **COMSOL**

## Split-gate device for indirect excitons

C. J. Dorow,<sup>1,a)</sup> J. R. Leonard,<sup>1</sup> M. M. Fogler,<sup>1</sup> L. V. Butov,<sup>1</sup> K. W. West,<sup>2</sup> and L. N. Pfeiffer<sup>2</sup>

<sup>1</sup>Department of Physics, University of California at San Diego, La Jolla, California 92093, USA

<sup>2</sup>Department of Electrical Engineering, Princeton University, Princeton, New Jersey 08544, USA

(Received 4 January 2018; accepted 9 March 2018; published online 30 April 2018)

We present a concept and experimental proof of principle for split-gate devices for indirect excitons (IXs). The split-gate forms a narrow channel, a point contact, for IX current. Control of IX flow through the split-gate with both gate voltage and excitation power is demonstrated. *Published by AIP Publishing.* <https://doi.org/10.1063/1.5021488>

Split-gates can be utilized for creating and controlling narrow channels (quantum point contacts) for electrons in mesoscopic electronic devices. Studies of electronic split-gate devices have led to a number of findings including electron focusing,<sup>1–4</sup> conductance quantization,<sup>5,6</sup> electron beam collimation,<sup>7–9</sup> and electron flow branching.<sup>10,11</sup>

In this work, we present a concept and proof-of-principle experiments with split-gate devices for indirect excitons (IXs). An IX is a bound pair of an electron and a hole in spatially separated layers, which can be realized in coupled quantum well (CQW) structures [Fig. 1(a)]. Due to several advantageous properties, IXs form a system that can be used to explore transport of cold bosons through split-gate devices, providing a counterpart to the many transport studies of cold fermions through electronic split-gate devices. These properties include the following: (i) IXs have built-in dipole moments  $ed$ , allowing the control of IX energy by voltage, where the IX energy shifts as  $\delta E = -edF_z$  ( $d$  is the separation between the electron and hole layers, and  $F_z$  is the voltage controllable electric field in the structure growth direction). Various in-plane potential landscapes formed by voltage for IXs were studied in earlier works, including excitonic ramps,<sup>12–14</sup> static<sup>15–19</sup> and moving<sup>20</sup> lattices, traps,<sup>21–26</sup> and transistors.<sup>27</sup> (ii) Long IX lifetimes allow them to travel long distances in mesoscopic devices before recombination.<sup>12–14,18–20,27</sup> (iii) Long IX lifetimes also allow effective IX thermalization with the crystal lattice,<sup>28</sup> giving the opportunity to study IX transport through mesoscopic devices in the quantum regime below the temperature of quantum degeneracy.

An excitonic split-gate device is formed by two electrodes: a large electrode [shown in blue (dark) in Fig. 1(b)] and a split-gate electrode [shown in gray in Fig. 1(b)]. Voltage  $V_e$  on the large electrode realizes the indirect regime in which IXs form the lowest energy state with energies below the energy of spatially direct excitons (DXs), which is also shown in Fig. 1(a). Gate voltage  $V_g$  on the split-gate electrode creates a narrow channel for IXs [Figs. 1(c)–1(f)]. The design of the IX split-gate device is similar to the design of electronic split-gate devices in semiconductor structures.<sup>4–11</sup> A difference is in the presence of the large electrode, which is needed to implement the indirect regime for IX devices. This large electrode is separated from the split-gate electrode by a narrow opening. We note that in some IX CQW

samples, e.g., in GaAs/AlAs CQW samples studied in Refs. 12, 17, and 21, the indirect regime is realized at  $V_e = 0$ . Therefore, these samples do not require a large electrode and, in turn, the narrow opening between it and the split-gate electrode, making the device design simpler.

The electric field  $F_z(x, y)$  and resulting IX potential energy  $U_{\text{bare}}(x, y) = -edF_z(x, y)$  for the bare, unscreened, split-gate device were modeled by numerically solving Poisson's equation (note that the split-gate potential landscape and, in turn,  $w$  are affected by IX screening, which is discussed below). Cross-sections of IX energy profiles at the split-gate position are shown in Fig. 1(c) for different  $V_g$  values. The IX energy is given relative to the energy of IXs far from the split-gate electrode, as determined by  $V_e$  on the large electrode.

The channel width  $w$  for transport of IXs with energy  $E$  (relative to the IX energy in a bare device away from the split-gate) is controlled by  $V_g$ . This is illustrated in Fig. 1(d) for a bare potential for several  $E$  values. The control of the split-gate channel by voltage provides control of IX current passing through. At low temperatures,  $E$  is determined by IX interaction. IXs are oriented dipoles and interact repulsively with the interaction energy on the order of meV for typical IX densities.<sup>19,29</sup> The IX interaction energy for IX split-gate devices is analogous to the electron Fermi energy for electronic split-gate devices.

Figures 1(e) and 1(f) present 3D images illustrating IX transport through a split-gate. IXs are generated by laser excitation on one side of the split-gate device [laser excitation centered around  $y = -5 \mu\text{m}$  is shown in Fig. 1(f)] and travel to the other side through the split-gate. This geometry corresponds to the experiments described below.

In the CQW structure grown by molecular beam epitaxy, an  $n^+$ -GaAs layer with  $n_{\text{Si}} = 10^{18} \text{ cm}^{-3}$  serves as a homogeneous bottom electrode. Two 8 nm GaAs QWs are separated by a 4 nm  $\text{Al}_{0.33}\text{Ga}_{0.67}\text{As}$  barrier and positioned  $0.1 \mu\text{m}$  above the  $n^+$ -GaAs layer within an undoped  $1 \mu\text{m}$  thick  $\text{Al}_{0.33}\text{Ga}_{0.67}\text{As}$  layer. The QWs are positioned close to the homogeneous bottom electrode to suppress the in-plane electric field,<sup>17</sup> which could otherwise lead to IX dissociation.<sup>15</sup> The top semitransparent electrodes are fabricated by applying 2 nm Ti and 7 nm Pt.

IXs were generated by a 633 nm HeNe laser focused to a spot with a full width half maximum of  $\sim 5 \mu\text{m}$ . Exciton photoluminescence (PL) was measured using a spectrometer and

<sup>a)</sup>Electronic mail: cdorow@physics.ucsd.edu

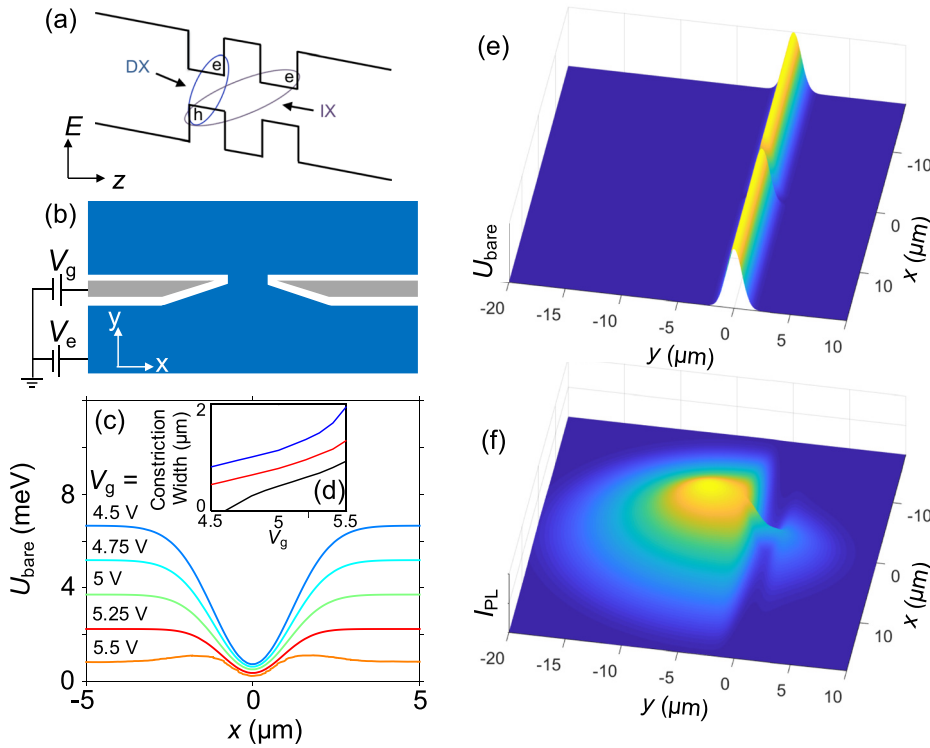


FIG. 1. (a) CQW band diagram. The ovals indicate a direct exciton (DX) and an indirect exciton (IX) composed of an electron ( $e$ ) and a hole ( $h$ ). (b) Schematic of the excitonic split-gate device. (c) Simulated bare constriction energy profiles for different split-gate voltages  $V_g$  for fixed voltage on the large electrode,  $V_e = 5.5$  V. (d) The corresponding constriction width  $w$  for IXs with different energies of  $E = 0.5$  (black),  $0.7$  (red), and  $1$  meV (blue) vs  $V_g$ . (e) Simulated IX potential energy in the bare split-gate device. (f) Simulated IX PL in potential of (e).

a liquid nitrogen cooled charge coupled device camera (CCD). The spatial  $x$ - $y$  IX PL pattern was measured using the CCD after spectral selection by an  $800 \pm 5$  nm interference filter chosen to match the IX energy. As a result, the low-energy bulk emission, higher-energy DX emission, and scattered laser light were effectively removed and the IX PL images were visualized. Experiments were performed in an optical helium cryostat at a bath temperature of  $T_{\text{bath}} = 1.7$  K.

Experimental proof of principle for the IX split-gate device is shown in Fig. 2. IXs are photogenerated on one side of the split-gate [the laser is positioned at  $(0, -4 \mu\text{m})$  in Fig. 2], and their transport through the split-gate is detected by measuring the spatial pattern of the IX emission. The rows in Fig. 2(a) and Figs. 2(b) and 2(d) show control of IX transport through the split-gate by gate voltage  $V_g$  for a fixed laser excitation power  $P$ . Increasing the channel width  $w$  by voltage enhances the IX flux through the split-gate.

The columns in Fig. 2(a) and Figs. 2(c) and 2(e) show control of IX transport through the split-gate by laser excitation power  $P$  for a fixed gate voltage  $V_g$ . Increasing IX density by excitation power enhances the IX flux through the split-gate. This is described in terms of screening below.

We simulated IX transport through the split-gate in the diffusive regime corresponding to the proof of principle experiments shown in Fig. 2. This regime is characterized by the mean free path small compared to the device dimensions. The following nonlinear partial differential equation was used to model IX transport through the split-gate:

$$\nabla \cdot [D\nabla n + \mu n \nabla (u_0 n + U_{\text{bare}})] + \Lambda_0 - \frac{n}{\tau} = 0. \quad (1)$$

The first term in square brackets in Eq. (1) accounts for IX diffusion,  $n$  is the IX density, and  $D$  is the IX diffusion coefficient.

The second term accounts for IX drift due to the dipole-dipole IX interaction, which is approximated by the plate capacitor formula  $u_0 n = \frac{4\pi e^2 d}{\epsilon} n$ ,  $\epsilon$  is the dielectric constant,<sup>29</sup> and due to the split-gate potential,  $U_{\text{bare}}(x, y) = -e d F_z(x, y)$ . The IX mobility  $\mu$  is given by the Einstein relation  $\mu = D/(k_B T)$ . The effect of in-plane disorder intrinsic to QWs is approximated using a “thermionic model” for the diffusion coefficient,  $D = D^{(0)} \exp(-U_{\text{dis}}/(k_B T + u_0 n))$ .<sup>29</sup>  $D^{(0)}$  is the diffusion coefficient in the absence of QW disorder, and  $U_{\text{dis}}/2$  is the amplitude of the disorder potential. The temperature of IXs  $T$  is approximated as  $T = T_{\text{bath}}$ . The non-resonant photoexcitation causes heating of the IX gas by a few Kelvin. However, the hot IXs cool to the lattice temperature within a few microns of the excitation spot,<sup>30</sup> justifying the approximation. The last two terms in Eq. (1) account for the creation and decay of IXs.  $\Lambda_0(x, y)$  is the IX generation rate and  $\tau$  is the IX lifetime.

Simulations (Fig. 3) qualitatively reproduce the control of IX transport through the split-gate both by voltage  $V_g$  [compare Fig. 2(b) with Fig. 3(a) and Fig. 2(d) with Fig. 3(b)] and by excitation power  $P$  [compare Fig. 2(c) with Fig. 3(c) and Fig. 2(e) with Fig. 3(d)]. The data are discussed below.

Increasing the absolute value of gate voltage  $V_g$  increases the channel width  $w$  at the IX energy and also reduces the barrier height [Fig. 1(c)]. As a result, IX transport through the split-gate is controlled by gate voltage  $V_g$  [rows in Fig. 2(a) and Figs. 2(b), 2(d), 3(a), and 3(b)]. The dependence on voltage in simulations is presented by the dependence on the height of the bare barrier away from the channel  $A_{\text{barrier}}$  [e.g.  $A_{\text{barrier}} = 3$  meV corresponds to  $V_g = 5.1$  V, see Fig. 1(c)].

Increasing IX excitation power  $P$  increases IX density  $n$ . This causes screening of the split-gate potential by IXs, increasing the channel width and reducing the barrier for IX transport through the split-gate [Figs. 3(e) and 3(f)]. Increasing  $n$  also causes screening of disorder as IXs interact

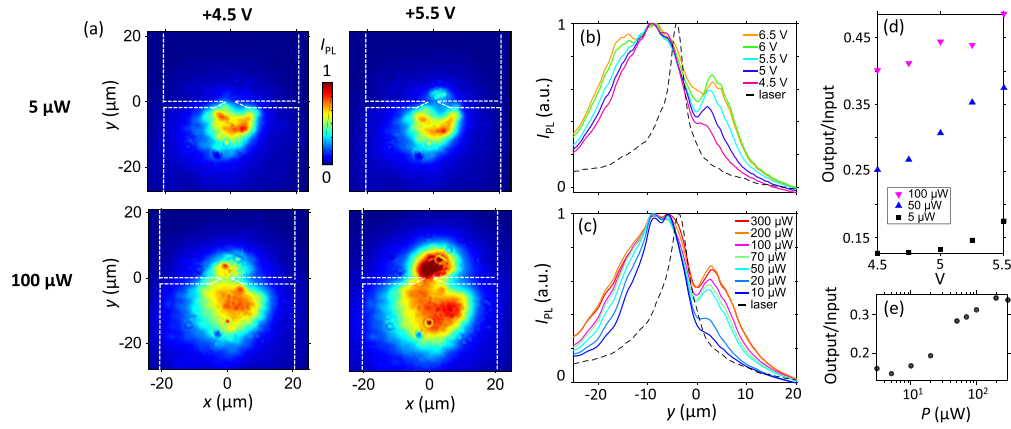


FIG. 2. (a) IX PL emission for two split-gate voltages  $V_g = 4.5$  and  $5.5$  V and two laser excitation powers  $P = 5$  and  $100 \mu\text{W}$ . The contour of the large electrode is shown with dashed lines. (b) Normalized IX PL intensity integrated over  $x$  vs  $V_g$ ,  $P = 50 \mu\text{W}$ . (c) Normalized IX PL intensity integrated over  $x$  vs  $P$ ,  $V_g = 4.5$  V. (d) IX flux through constriction vs  $V_g$ ,  $P = 5, 50,$  and  $100 \mu\text{W}$ . (e) IX flux through constriction vs  $P$ ,  $V_g = 4.5$  V. The large electrode is held at  $V_e = 5.5$  V for all data.

repulsively. Screening of the split-gate potential and disorder increases IX transport through the split-gate [columns in Fig. 2(a) and Figs. 2(c), 2(e), 3(c), and 3(d)].

Note that in the experiment, the peak of the PL does not correspond to the peak of the laser. This feature is related to the inner ring effect caused by PL suppression in the region of the laser excitation spot due to temperature enhancement.<sup>30</sup> This effect is not observed in the simulations, where the IX temperature is approximated as  $T = T_{\text{bath}}$ .

An interesting regime for electron transport through electronic split-gates is the regime of quantum ballistic transport, where the mean free path and Fermi wavelength exceed the device dimensions. This regime is realized for electronic

split-gate devices in high-quality semiconductor structures at low temperatures.<sup>4–11</sup>

For excitonic devices, at low temperatures ( $T \sim 0.1$  K, achievable in dilution refrigerators<sup>28,31</sup>), the IX coherence length in a coherent IX gas in high-quality CQW semiconductor structures reaches  $\sim 10 \mu\text{m}$ ,<sup>31</sup> exceeding the dimensions of the split-gate channel (Fig. 1), IX interparticle separation ( $\sim 0.1 \mu\text{m}$  for a typical IX density of  $10^{10} \text{cm}^{-2}$ ), and IX thermal de Broglie wavelength ( $\sim 0.5 \mu\text{m}$  for an IX temperature of  $T = 0.1$  K). This indicates the feasibility of the realization of IX quantum ballistic transport through excitonic split-gate devices at low temperatures. The realization of this regime forms the subject for future works.

We note that excitonic split-gate devices allow imaging IX current paths after spatially localized IX injection. Therefore, besides giving the opportunity to extend studies of narrow-channel phenomena in fermions<sup>1–11</sup> to bosons, IX split-gate devices can also be used as a tool to probe directional effects in transport of composite bosons, including the predicted exciton Hall effect<sup>32</sup> and exciton spin Hall effect.<sup>33</sup> Excitonic split-gate devices can also be used for studying transport of composite particles through narrow channels.<sup>34</sup>

In conclusion, we presented a concept and experimental proof of principle for split-gate devices for indirect excitons.

This work was supported by NSF Grant No. 1640173 and NERC, a subsidiary of SRC, through the SRC-NRI Center for Excitonic Devices. C.J.D. was supported by the NSF Graduate Research Fellowship Program under Grant No. DGE-1144086. This work used the Extreme Science and Engineering Discovery Environment (XSEDE), which was supported by NSF Grant No. ACI-1548562, and XSEDE computer Comet at the San Diego Supercomputer Center through allocation TG-ASC150024.

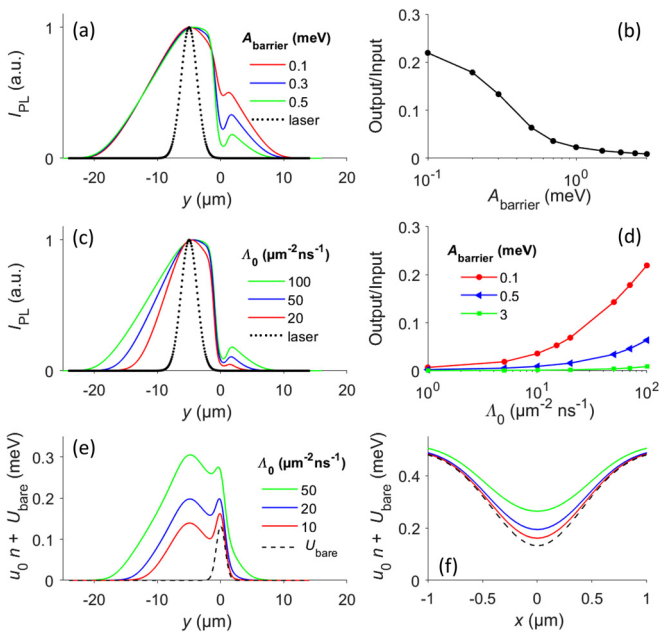


FIG. 3. Results of simulations. (a) IX PL vs bare barrier height  $A_{\text{barrier}}$ . IX generation rate  $\Lambda_0 = 100 \mu\text{m}^{-2} \text{ns}^{-1}$ . IX PL is integrated over  $x$ . The laser profile is indicated with a dotted line. Data correspond to  $V_g = 5.7$  V ( $A_{\text{barrier}} = 0.1$  meV),  $V_g = 5.66$  V ( $A_{\text{barrier}} = 0.3$  meV), and  $V_g = 5.63$  V ( $A_{\text{barrier}} = 0.5$  meV). (b) IX flux through constriction vs  $A_{\text{barrier}}$ ,  $\Lambda_0 = 100 \mu\text{m}^{-2} \text{ns}^{-1}$ . (c) IX PL vs  $\Lambda_0$ ,  $A_{\text{barrier}} = 0.5$  meV. IX PL is integrated over  $x$ . (d) IX flux through constriction vs  $\Lambda_0$ ,  $A_{\text{barrier}} = 0.1, 0.5,$  and  $3$  meV. (e) IX energy  $U_0 n + U_{\text{bare}}$  vs  $y$  at  $x = 0$  and (f) vs  $x$  at  $y = 0$  for several  $\Lambda_0$  values. The bare barrier profile  $U_{\text{bare}}$  is shown by dashed lines.  $A_{\text{barrier}} = 0.5$  meV. For all simulations,  $T_{\text{bath}} = 1.7$  K.

<sup>1</sup>Y. V. Sharvin, “A possible method for studying Fermi surfaces,” *J. Exp. Theor. Phys.* **48**, 984–985 (1965) [*Sov. Phys. JETP* **21**, 655–656 (1965)].

<sup>2</sup>Y. V. Sharvin and L. M. Fisher, “Observation of focused electron beams in a metal,” *Pisma ZhETF* **1**, 54–57 (1965) [*JETP Lett.* **1**, 152–153 (1965)].

<sup>3</sup>V. S. Tsoi, “Focusing of electrons in a metal by a transverse magnetic field,” *Pisma ZhETF* **19**, 114–116 (1974) [*Pisma JETP* **19**, 70–71 (1974)].

- <sup>4</sup>H. van Houten, B. J. van Wees, J. E. Mooij, C. W. J. Beenakker, J. G. Williamson, and C. T. Foxon, "Coherent electron focussing in a two-dimensional electron gas," *Europhys. Lett.* **5**, 721–725 (1988).
- <sup>5</sup>B. J. van Wees, H. van Houten, C. W. J. Beenakker, J. G. Williamson, L. P. Kouwenhoven, D. van der Marel, and C. T. Foxon, "Quantized conductance of point contacts in a two-dimensional electron gas," *Phys. Rev. Lett.* **60**, 848–850 (1988).
- <sup>6</sup>D. A. Wharam, T. J. Thornton, R. Newbury, M. Pepper, H. Ahmed, J. E. F. Frost, D. G. Hasko, D. C. Peacock, D. A. Ritchie, and G. A. C. Jones, "One-dimensional transport and the quantisation of the ballistic resistance," *J. Phys. C: Solid State Phys.* **21**, L209–L214 (1988).
- <sup>7</sup>L. W. Molenkamp, A. A. M. Staring, C. W. J. Beenakker, R. Eppenga, C. E. Timmering, J. G. Williamson, C. J. P. M. Harmans, and C. T. Foxon, "Electron-beam collimation with a quantum point contact," *Phys. Rev. B* **41**, 1274–1277 (1990).
- <sup>8</sup>M. A. Eriksson, R. G. Beck, M. Topinka, J. A. Katine, R. M. Westervelt, K. L. Campman, and A. C. Gossard, "Cryogenic scanning probe characterization of semiconductor nanostructures," *Appl. Phys. Lett.* **69**, 671–673 (1996).
- <sup>9</sup>R. Crook, C. G. Smith, C. H. W. Barnes, M. Y. Simmons, and D. A. Ritchie, "Imaging diffraction-limited electronic collimation from a non-equilibrium one-dimensional ballistic constriction," *J. Phys.: Condens. Matter* **12**, L167–L172 (2000).
- <sup>10</sup>M. A. Topinka, B. J. LeRoy, S. E. J. Shaw, E. J. Heller, R. M. Westervelt, K. D. Maranowski, and A. C. Gossard, "Imaging coherent electron flow from a quantum point contact," *Science* **289**, 2323–2326 (2000).
- <sup>11</sup>M. A. Topinka, B. J. LeRoy, R. M. Westervelt, S. E. J. Shaw, R. Fleischmann, E. J. Heller, K. D. Maranowski, and A. C. Gossard, "Coherent branched flow in a two-dimensional electron gas," *Nature* **410**, 183–188 (2001).
- <sup>12</sup>M. Hagn, A. Zrenner, G. Böhm, and G. Weimann, "Electric-field-induced exciton transport in coupled quantum well structures," *Appl. Phys. Lett.* **67**, 232–234 (1995).
- <sup>13</sup>A. Gärtner, A. W. Holleitner, J. P. Kotthaus, and D. Schuh, "Drift mobility of long-living excitons in coupled GaAs quantum wells," *Appl. Phys. Lett.* **89**, 052108 (2006).
- <sup>14</sup>C. J. Dorow, Y. Y. Kuznetsova, J. R. Leonard, M. K. Chu, L. V. Butov, J. Wilkes, M. Hanson, and A. C. Gossard, "Indirect excitons in a potential energy landscape created by a perforated electrode," *Appl. Phys. Lett.* **108**, 073502 (2016).
- <sup>15</sup>S. Zimmermann, A. O. Govorov, W. Hansen, J. P. Kotthaus, M. Bichler, and W. Wegscheider, "Lateral superlattices as voltage-controlled traps for excitons," *Phys. Rev. B* **56**, 13414–13421 (1997).
- <sup>16</sup>S. Zimmermann, G. Schedelbeck, A. O. Govorov, A. Wixforth, J. P. Kotthaus, M. Bichler, W. Wegscheider, and G. Abstreiter, "Spatially resolved exciton trapping in a voltage-controlled lateral superlattice," *Appl. Phys. Lett.* **73**, 154–156 (1998).
- <sup>17</sup>A. T. Hammack, N. A. Gippius, S. Yang, G. O. Andreev, L. V. Butov, M. Hanson, and A. C. Gossard, "Excitons in electrostatic traps," *J. Appl. Phys.* **99**, 066104 (2006).
- <sup>18</sup>M. Remeika, M. M. Fogler, L. V. Butov, M. Hanson, and A. C. Gossard, "Two-dimensional electrostatic lattices for indirect excitons," *Appl. Phys. Lett.* **100**, 061103 (2012).
- <sup>19</sup>M. Remeika, J. R. Leonard, C. J. Dorow, M. M. Fogler, L. V. Butov, M. Hanson, and A. C. Gossard, "Measurement of exciton correlations using electrostatic lattices," *Phys. Rev. B* **92**, 115311 (2015).
- <sup>20</sup>A. G. Winbow, J. R. Leonard, M. Remeika, Y. Y. Kuznetsova, A. A. High, A. T. Hammack, L. V. Butov, J. Wilkes, A. A. Guenther, A. L. Ivanov, M. Hanson, and A. C. Gossard, "Electrostatic conveyer for excitons," *Phys. Rev. Lett.* **106**, 196806 (2011).
- <sup>21</sup>T. Huber, A. Zrenner, W. Wegscheider, and M. Bichler, "Electrostatic exciton traps," *Phys. Status Solidi A* **166**, R5–R6 (1998).
- <sup>22</sup>A. V. Gorbunov and V. B. Timofeev, "Interwell excitons in a lateral potential well in an inhomogeneous electric field," *JETP Lett.* **80**, 185–189 (2004) [*Pisma Zh. Eksp. Teor. Fiz.* **80**, 210–215 (2004)].
- <sup>23</sup>A. A. High, A. T. Hammack, L. V. Butov, L. Mouchliadis, A. L. Ivanov, M. Hanson, and A. C. Gossard, "Indirect excitons in elevated traps," *Nano Lett.* **9**, 2094–2098 (2009).
- <sup>24</sup>G. J. Schinner, J. Repp, E. Schubert, A. K. Rai, D. Reuter, A. D. Wieck, A. O. Govorov, A. W. Holleitner, and J. P. Kotthaus, "Confinement and interaction of single indirect excitons in a voltage-controlled trap formed inside double InGaAs quantum wells," *Phys. Rev. Lett.* **110**, 127403 (2013).
- <sup>25</sup>Y. Shilo, K. Cohen, B. Laikhtman, K. West, L. Pfeiffer, and R. Rapaport, "Particle correlations and evidence for dark state condensation in a cold dipolar exciton fluid," *Nat. Commun.* **4**, 2335 (2013).
- <sup>26</sup>Y. Mazuz-Harpaz, K. Cohen, B. Laikhtman, R. Rapaport, K. West, and L. N. Pfeiffer, "Radiative lifetimes of dipolar excitons in double quantum wells," *Phys. Rev. B* **95**, 155302 (2017).
- <sup>27</sup>P. Andreakou, S. V. Poltavtsev, J. R. Leonard, E. V. Calman, M. Remeika, Y. Y. Kuznetsova, L. V. Butov, J. Wilkes, M. Hanson, and A. C. Gossard, "Optically controlled excitonic transistor," *Appl. Phys. Lett.* **104**, 091101 (2014).
- <sup>28</sup>L. V. Butov, A. L. Ivanov, A. Imamoglu, P. B. Littlewood, A. A. Shashkin, V. T. Dolgoplov, K. L. Campman, and A. C. Gossard, "Stimulated scattering of indirect excitons in coupled quantum wells: signature of a degenerate Bose-gas of excitons," *Phys. Rev. Lett.* **86**, 5608–5611 (2001).
- <sup>29</sup>A. L. Ivanov, "Quantum diffusion of dipole-oriented indirect excitons in coupled quantum wells," *Europhys. Lett.* **59**, 586–591 (2002).
- <sup>30</sup>A. T. Hammack, L. V. Butov, J. Wilkes, L. Mouchliadis, E. A. Muljarov, A. L. Ivanov, and A. C. Gossard, "Kinetics of the inner ring in the exciton emission pattern in coupled GaAs quantum wells," *Phys. Rev. B* **80**, 155331 (2009).
- <sup>31</sup>A. A. High, J. R. Leonard, A. T. Hammack, M. M. Fogler, L. V. Butov, A. V. Kavokin, K. L. Campman, and A. C. Gossard, "Spontaneous coherence in a cold exciton gas," *Nature* **483**, 584–588 (2012).
- <sup>32</sup>A. B. Dzyubenko and Y. E. Lozovik, "Quasi two-dimensional electron-hole pair condensate in a strong magnetic field," *Fiz. Tverd. Tela* **26**, 1540–1541 (1984), [*Sov. Phys. Solid State* **26**, 938 (1984)].
- <sup>33</sup>A. Kavokin, G. Malpuech, and M. Glazov, "Optical spin Hall effect," *Phys. Rev. Lett.* **95**, 136601 (2005).
- <sup>34</sup>F. Grasselli, A. Bertoni, and G. Goldoni, "Exact two-body quantum dynamics of an electron-hole pair in semiconductor coupled quantum wells: A time-dependent approach," *Phys. Rev. B* **93**, 195310 (2016).

Copyright 2018 AIP Publishing. This article may be downloaded for personal use only. Any other use requires prior permission of the author and AIP Publishing.

The following article appeared in **Appl. Phys. Lett.** **112**, 183501 (2018)  
and may be found at <https://aip.scitation.org/doi/10.1063/1.5021488>